A High-Resolution Analytical Thermal Modeling Method of Capacitor Bank Considering Thermal Coupling and Different Cooling Modes

Chunlin Lv, *Graduate Student Member, IEEE*, Jinjun Liu, *Fellow, IEEE*, Yan Zhang, *Member, IEEE*, Jinpeng Yin, and Xiaotong Zhang

***Abstract*—Thermal stress is of crucial importance to capacitor reliability. However, for a capacitor bank, on spatial scale, the complex heat transfer modes are not clearly illustrated; and on time scale, the equivalent series resistance (ESR) aging is neither fully discussed in current evaluation methods. These could lead to a glaring error in the prediction of temperature distribution and lifetime estimation. Therefore, this article proposed an analytical thermal modeling method with high-resolution for the capacitor bank, considering the thermal coupling effect between individual capacitors, as well as different cooling conditions and the heat variation caused by ESR aging. First, the improved thermal state-space modeling method is proposed to universally describe a multiple heat source system. Then, based on heat transfer and fluid mechanic theories, the characterization method of thermal coupling effect in different cooling modes is discussed. Furthermore, the ESR aging model is applied in the electrothermal analysis of capacitor bank, aiming to improve the accuracy of thermal calculation in long time scale. Finally, to alleviate the uneven temperature distribution in an in-line designed capacitor bank, a staggered design method is proposed followed by a case study, where a nine-capacitor bank is presented to validate the corresponding modeling method and optimization.**

***Index Terms*—Aging, analytical thermal modeling, capacitor bank, capacitor optimization design, heat transfer, thermal coupling.**

I. Introduction

CAPACITORS are widely used in power electronics for smooth filtering, ripple current absorption, bypass, decoupling and storage [1]. For some applications where a single capacitor cannot fulfill the voltage rating or capacitance requirements, the capacitor bank is always used as the energy buffer by connecting several capacitors in parallel for larger capacitance or in series for higher voltage rating [2]. However, surveys show that capacitors are regarded as one of the most vulnerable devices in power electronics applications [3].

In order to accurately predict the health status of capacitor bank and to make reasonable maintenance strategies, the failure mechanisms of capacitors are explored deeply [1], [4], [5], [6], [7]. The reliability evaluation methods based on physics of failure model [8], [9], [10] and the data-driven remaining useful life (RUL) prediction methods [7], [11], [12] are proposed. For the former one, the influence of electrical stress on failure is represented by inverse power model, and the influence of thermal stress on failure is represented by Arrhenius formula. The latter one uses AI tools to establish the relationship between state parameters and reliability through data learning.

The key to successful reliability evaluation by these two methods is accurately obtaining the electrical stress and the thermal stress of capacitors. For electrical stress, the capacitor voltage can be calculated by circuit model and ripple current can be approximately obtained by current reconstruction method [13]. However, for thermal stress, there is no general method that can balance the accuracy and rapidity of calculation.

Thermal stress calculation is generally realized by a simplified one-dimensional (1-D) thermal network model. [14] This method can simulate the thermal behavior of a single capacitor in natural heat dissipation. However, in this way, it is not able to cope with different cooling conditions, neither it is capable of handling capacitor bank with multiheat source coupling in practical applications.

To solve this problem, a finite-element method (FEM) based on numerical calculation is proposed and developed. [15] This method subdivides the target system into smaller parts by space discretization, and then turns each finite element into a series of algebraic equations over the given boundary, finally the whole system is modeled by assembling all the parts. In this way, the temperature distribution over the whole region can be obtained. However, FEM requires a high amount of calculation. A more accurate result often requires more time consumption. Therefore, it is difficult to track temperature change by applying this method in a long-time scale mission profile. Given the above, for thermal stress analysis, there is an urgent need of finding a compromise between the calculation accuracy and efficiency.

Wang [2] paid attention to the problem of uneven temperature distribution in the multicapacitor bank and proposed thermal

Manuscript received 30 September 2022; revised 1 January 2023; accepted 10 February 2023. Date of publication 16 February 2023; date of current version 20 April 2023. This work was supported by the National Key Research and Development Plan under Grant 2018YFB0905800. Recommended for publication by Associate Editor F. Khan. *(Corresponding author: Chunlin Lv.)*

The authors are with the State Key Laboratory of Electrical Insulation and Power Equipment, School of Electrical Engineering, Xi'an Jiaotong University, Xi'an 710049, China (e-mail: lvchunlin@stu.xjtu.edu.cn; jjliu@mail.xjtu.edu.cn; zhangyanjtu@163.com; 841522097@qq.com; zxt200@stu.xjtu.edu.cn).

Color versions of one or more figures in this article are available at https://doi.org/10.1109/TPEL.2023.3245629.

Digital Object Identifier 10.1109/TPEL.2023.3245629

state-space modeling, which considered the thermal coupling between individuals that is neglected by conventional thermal network method. Nevertheless, it could not fully model the coupling between thermal field and fluid field, and did not involve the influence of aging in the heat production.

Based on this, an analytical thermal modeling method of capacitor bank with high temporal and spatial resolution is proposed in this article. On the spatial scale, the thermodynamic state-space modeling is improved. The thermal coupling between capacitors and the coupling between thermal field and fluid field are characterized by physical heat transfer model. On the time scale, the effect of degradation on the electrothermal behavior inside the capacitor is characterized by the equivalent series resistance (ESR) aging model. Consequently, this method can be incorporated into current reliability evaluation process, with the aging state and mission profile of capacitors being updated iteratively to extract the hot-spot temperature. The results obtained will be more consistent with reality. In addition, the proposed method can offer a reference guide to the capacitor bank design and solve the problem of premature aging caused by uneven temperature distribution.

The rest of this article is arranged as follows: Section II presents the current reliability evaluation system and thermal stress calculation method. In Section III, a high-resolution analytical thermal modeling method of capacitor bank considering the thermal coupling between capacitors, the coupling between thermal and fluid fields as well as capacitor aging is presented. In Section IV, the effectiveness of the method is verified by experiments, and the superiority of the method is shown in comparison with FEM simulation and other analytical methods. In Section V, a new capacitor arrangement design is proposed to alleviate the uneven temperature distribution and verified by experiments. Finally, Section VI concludes this article.

II. Reliability Evaluation Method and the Thermal Modeling Requirements of Capacitor Bank

This section introduces the state-of-the-art capacitor reliability evaluation method and summarizes the requirements when realizing electrothermal stress analysis of capacitor bank by clarifying the pros and cons of the conventional methods.

A. Capacitor Reliability Evaluation Method

A lot of research has been carried out on lifetime prediction and reliability evaluation of capacitors and many effective theories are thus pushed forward [16], [17], [18], [19]. Among them, the reliability evaluation method considering variable stress condition and ESR aging shows the most consistency with the failure characteristics of capacitors under practical operating conditions [20].

According to the aging failure mechanisms of capacitors, thermal stress is the key factor affecting the lifetime. Under constant stress, the lifetime model [1] can be expressed as

$$L = L_{\mathrm{N}}\left(\frac{U}{U_{\mathrm{N}}}\right)^{-n} 2^{\frac{T_{\mathrm{N}}-T_{\mathrm{hs}}}{\alpha}} \tag{1}$$

Fig. 1. 1-D simplified thermal model of capacitors.

where L and L_N are the lifetime under the practical operating condition and rated condition, respectively. U and U_N are the voltage at the practical operating condition and rated condition, respectively. T_{hs} and T_N are the temperatures at the hot spot and rated condition, respectively. n and α are the voltage coefficient and temperature coefficient which can be measured by the accelerated aging test.

However, in practical industrial applications, the external and internal stresses of capacitor bank are constantly changing. The change of external stress includes environmental temperature, humidity, load, etc., while the internal change mainly includes the increase of actual electrothermal stress caused by ESR aging. According to the aging characteristics, the aging model of capacitor can be expressed as [21], [22]

$$\mathrm{ESR}(t) = \mathrm{ESR}(0) \cdot \exp\left[(D(0) \cdot \int_0^t 2^{\frac{T_{\mathrm{hs}}(t)}{\alpha}} dt\right] \tag{2}$$

where ESR (0) is the initial value of ESR without aging, D (0) is the initial value of aging coefficient independent of temperature and α is the temperature coefficient. These coefficients can also be measured by the accelerated aging test.

Subsequently, the reliability evaluation method in [20] quantifies the influence of ESR aging and varying stress mission profile on reliability through iterative calculation, and finally determines component failure through accumulative damage. It should be noted that the evaluation result depends on the calculation accuracy of thermal stress, in the meantime, calculating accumulative damage in different periods of life cycle requires high speed.

B. Conventional Thermal Stress Calculation Method

Conventional thermal stress calculation methods can be divided into two categories: 1-D thermal network model and finite element simulation. [14], [15]

The 1-D thermal network model simulates the heat transfer process of capacitor through the thermal resistance provided by the datasheet [23], [28], as shown in Fig. 1, which can be expressed as

$$T_{\mathrm{hs}} = T_a + P_{\mathrm{loss}}(R_{\mathrm{th}-hc} + R_{\mathrm{th}-ca})$$

$$P_{\mathrm{loss}} = \sum_i^{\mathrm{N}} [ESR(f_i) \times I_{rms}^2(f_i)]$$

$$\mathrm{ESR}(f_i) = R_s + \frac{\tan\delta_0}{2\pi f_i \cdot C} \tag{3}$$

where $T_{\rm hs}$ is the hot-spot temperature, T_a is the ambient temperature, $R_{\text{th-}hc}$ is the thermal resistance from hotspot to case, and $R_{\text{th-}ca}$ is the thermal resistance from case to ambient. $I_{\rm rms}(f_{\rm i})$ is the root-mean-square (rms) capacitor current at specified frequency f_i. N represents the Nth harmonic current, R_s represents the sum of all ohmic resistances inside the capacitor, $\tan\delta_0$ represents the dielectric dissipation factor [23].

Experimental results show that this method is suitable for a single capacitor when the cooling condition is strictly limited to natural heat dissipation. However, in industrial applications, capacitors are always connected in series and parallel in a capacitor bank. Hence, when there is heat exchange between each capacitor, this simple method is no longer applicable, let alone in the other occasions where forced air cooling is adopted.

Correspondingly, as is known, FEM is very suitable for solving the coupling problem of multiphysical fields through massive numerical calculation. By applying FEM simulation, the accurate temperature distribution of the capacitor bank under given working condition and its aging state can be obtained. However, this method costs heavily the calculation time to ensure accuracy. In some circumstances, it can take hours to complete a simulation, which seems not realistic to fulfill a long-time scale simulation of hot-spot temperature under varying stress condition and aging stages. Judging from above, it is hard to meet the need of an entire reliability evaluation process through FEM, considering mission profile and ESR aging.

C. Thermal Modeling Requirements of Capacitor Bank

To sum up, it is required a set of universal methods for capacitor bank thermal modeling, which can be used to obtain the hot-spot temperature distribution no matter what kind of arrangement, what cooling mode or what aging state. At the same time, it is necessary to improve the calculation efficiency on the premise of ensuring its accuracy, which means an acceptable fault tolerance.

III. Universal Analytical Thermal Modeling Method

In this section, an improved thermal stress calculation method, with high temporal and spatial resolution, is proposed for capacitor bank based on thermodynamic state-space modeling. It is committed to satisfying the modeling requirements mentioned in Section II, guaranteeing a good compromise between the accuracy and efficiency of the thermal stress analysis.

A. Improved Thermodynamic State-Space Modeling

According to the basic law of heat transfer, supposing that the temperature at two points a and b in space is T_a and T_b respectively, and the heat flow between the two is $P_{\rm loss}$. The thermal resistance between a and b can be defined as $R_{{\rm th},ab}$

$$R_{{\rm th},ab} = \frac{T_a - T_b}{P_{\rm loss}}. \tag{4}$$

A state-space modeling method has been proposed considering multi-heat source and time-varying non-linear coupling thermal resistance in a multicapacitor bank [2]. For capacitor i, the energy balance equation can be established at the case temperature node

$$C_{{\rm th},i}\frac{dT_{c,i}}{dt} = \sum_{j=1,j\neq {\rm i}}^{n}\frac{1}{R_{\rm th,ij}}(T_{c,j}-T_{c,i}) + P_{{\rm loss},i} \quad (i=1,\ldots,n) \tag{5}$$

where $P_{{\rm loss},i}$ represents the power loss injection related to the node. $T_{c,i}$ represents the case temperature. $R_{{\rm th},ij}$ represents the thermal resistance between cases. $C_{{\rm th},i}$ represents the equivalent thermal capacitance of the node.

When case temperature variation is equal to zero, the energy balance is reached. Then the hot-spot temperature can be calculated using the thermal resistance from the case to the hot spot provided in the datasheet.

To some extent, this method overcomes the difficulty in calculating the hot-spot temperature when there exists multiheat source coupling, which is not covered in 1-D thermal network model. However, the test results show that there is still a significant gap between the simulated temperature and the actual temperature. That is because the characterization of coupling thermal resistance is too simplified, resulting in a low spatial resolution. Further, such coupling analysis still has some restrictions, making it less sufficient to be applied in thermal analysis with more complex cooling conditions.

Therefore, in this article, the state-space modeling process is firstly updated, adding a supplement as the heat transfer from the case to the ambience far from the surface in the original equation. The improved model is shown as

$$\begin{aligned} C_{{\rm th},i}\frac{dT_{c,i}}{dt} = &\sum_{j=1,j\neq i}^{n}\frac{1}{R_{{\rm th},ij}}(T_{c,j}-T_{c,i}) \\ &+ \frac{1}{R_{\rm th,ia}}(T_a - T_{c,i}) + P_{{\rm loss},i}(t) \\ &(i=1,\ldots,n) \end{aligned} \tag{6}$$

where T_a is ambient temperature and $R_{{\rm th},ia}$ is thermal resistance from case to ambience far from the surface. For the capacitor bank with n order differential equations, the thermal dynamics of the case temperature can be expressed with a matrix representation

$$\boldsymbol{C_{th}}\frac{d\boldsymbol{T}_c}{dt} = \boldsymbol{AT} + \boldsymbol{BP}(t) \tag{7}$$

where $\boldsymbol{T}$ represents the temperature matrix consist of case temperature matrix $\boldsymbol{T_c}$ and ambient temperature T_a, $\boldsymbol{P}$(t) represents varying power loss injection considering aging effect which can be obtained by iterating the ESR aging according to (2) and (3), $\boldsymbol{A}$ represent the thermal resistance matrix, $\boldsymbol{B}$ represent the system matrix and $\boldsymbol{C_{\rm th}}$ represents the equivalent thermal capacitance matrix, which is ignored for the steady state temperature estimation.

In thermal resistance matrix $\boldsymbol{A}$, $R_{{\rm th},ij}$ is the coupling thermal resistance between capacitors, $R_{{\rm th},ia}$ is the self-heating thermal resistance from the case i to ambience far from the surface. The hot-spot temperature distribution of the capacitor bank can be derived as

$$T_{hs,i} = T_{c,i} + R_{{\rm th},hc,i}P_{{\rm loss},i}(t) \tag{9}$$

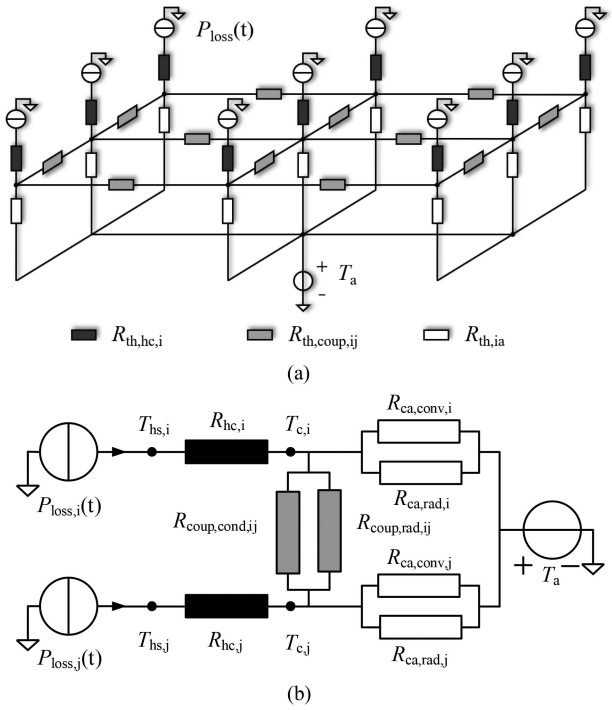

Fig. 2. Analytical thermal model of capacitor bank with thermal coupling. (a) Capacitor bank. (b) Adjacent two capacitors.

where $R_{\mathrm{th},hc,i}$ is the thermal resistance from the hot-spot to case i and $T_{hs,i}$ is the hot-spot temperature of the capacitor i. The major challenge is to identify the thermal matrix $\boldsymbol{A}$ in (8) shown at the bottom of this page, for different capacitor bank layouts and heat dissipation conditions, of which the characterization is clarified in the following parts, to raise the spatial resolution.

In addition, this model takes into account the thermal energy variation caused by the increase of capacitor ESR in long-term operation, which allows not only to calculate the steady-state hot-spot temperature in short-time scale, but also to track the dynamic change of hot-spot temperature in long time scale, where a significant improvement is seen in the temporal resolution.

This model is shown in Fig. 2, where the black blocks indicate the thermal resistance from hot spot to case, the white blocks indicate the thermal resistance from case to ambient far from the surface and the grey blocks indicate coupling thermal resistance between adjacent two capacitors.

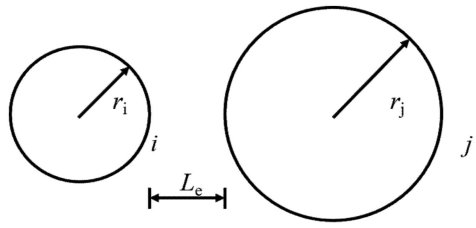

Fig. 3. Description of coupling view factor between capacitors.

B. Characterization of Coupling Thermal Resistance

According to the basic principles of heat transfer [24], the coupling thermal resistance between capacitors consists of conduction and radiation thermal resistance as shown in Fig. 2.

Conduction thermal resistance can be expressed as

$$R_{\mathrm{coup,cond},ij} = \frac{L_e}{kAF_{ij}} \tag{10}$$

where L_e is the equivalent heat conduction distance. k is the thermal conductivity of air. A is the heat transfer surface area of individual capacitor. F_{ij} is the coupling view factor between capacitors, which can be written as [25]. For capacitors, the shape is generally cylindrical and F_{ij} can be expressed as (11), which is shown in Fig. 3

$$\begin{aligned} F_{ij} = \frac{1}{2\pi}\Bigg(\pi + \Big(C^2-(R+1)^2\Big)^{1/2} - \Big(C^2-(R-1)^2\Big)^{1/2} \\ + (R-1)\arccos\left(\frac{R}{C}-\frac{1}{C}\right) - (R+1)\arccos\left(\frac{R}{C}+\frac{1}{C}\right)\Bigg) \end{aligned} \tag{11}$$

where $R = r_i/r_j$, $S = L_e/r_i$, $C = 1 + R + S$.

The radiation thermal resistance between any two gray, diffuse, opaque surfaces that form an enclosure is given by

$$R_{\mathrm{coup,rad},ij} = \frac{\frac{1-\varepsilon_i}{A_i\varepsilon_i} + \frac{1}{A_iF_{ij}} + \frac{1-\varepsilon_j}{A_j\varepsilon_j}}{\sigma(T_i^2+T_j^2)(T_i+T_j)} \tag{12}$$

where ε is the emissivity of the surface material. $\sigma = 5.670 \times 10^{-8}$ W/m^2·K^4 is the Stephan–Boltzman constant.

$$\boldsymbol{A} = \begin{bmatrix} -\sum_{j=2}^{n}\frac{1}{R_{\mathrm{th},ij}} - \frac{1}{R_{\mathrm{th},1a}} & \frac{1}{R_{\mathrm{th},12}} & \cdots & \frac{1}{R_{\mathrm{th},1n}} & \frac{1}{R_{\mathrm{th},1a}} \\ \frac{1}{R_{\mathrm{th},21}} & -\sum_{j=1,j\neq 2}^{n}\frac{1}{R_{\mathrm{th},ij}} - \frac{1}{R_{\mathrm{th},ia}} & \cdots & \frac{1}{R_{\mathrm{th},2n}} & \frac{1}{R_{\mathrm{th},2a}} \\ \cdots & \cdots & \cdots & \cdots & \cdots \\ \frac{1}{R_{\mathrm{th},n1}} & \frac{1}{R_{\mathrm{th},n2}} & \cdots & -\sum_{j=1}^{n-1}\frac{1}{R_{\mathrm{th},ij}} - \frac{1}{R_{\mathrm{th},na}} & \frac{1}{R_{\mathrm{th},na}} \end{bmatrix}$$

$$\boldsymbol{T} = \begin{bmatrix} T_{c,1} \\ T_{c,2} \\ \cdots \\ T_{c,n} \\ T_a \end{bmatrix} \quad \boldsymbol{P}(t) = \begin{bmatrix} P_{\mathrm{loss},1}(t) \\ P_{\mathrm{loss},2}(t) \\ \cdots \\ P_{\mathrm{loss},n}(t) \end{bmatrix} \quad \boldsymbol{B} = \begin{bmatrix} 1 & 0 & \cdots & 0 \\ 0 & 1 & \cdots & 0 \\ \cdots & \cdots & \cdots & \cdots \\ 0 & 0 & 0 & 1 \end{bmatrix} \tag{8}$$

C. Characterization of Thermal Resistance From Case to Ambience Far From the Surface

According to the basic principles of heat transfer [24], the thermal resistance from case to ambience far from the surface consists of convection and radiation thermal resistance as shown in Fig. 2.

The convection thermal resistance between case *i* and ambience far from the surface can be expressed as

$$R_{\mathrm{conv},ia} = \frac{1}{hA} \tag{13}$$

where *h* is the convection heat transfer coefficient, which can be written as

$$h = \mathrm{Nu}\frac{k}{L_c} \tag{14}$$

where Nu is the Nusselt number and L_c is the characteristic length of the geometry. Flows across cylinders, in general, involve flow separation, which is difficult to handle analytically. Therefore, such flows must be studied experimentally or numerically. This article has compared different empirical correlations and adopted the highest accuracy one.

For natural cooling, Nu can be expressed as [24]

$$\mathrm{Nu} = \left\{0.825 + \frac{0.387\mathrm{Ra}_D^{1/6}}{\left[1+\left(\frac{0.492}{\mathrm{Pr}}\right)^{9/16}\right]^{8/27}}\right\}^2 \tag{15}$$

where $\mathrm{Ra_D}$ is the Rayleigh number and Pr is the Prandtl number

$$\mathrm{Ra}_D = \frac{g\beta(T_s - T_\infty)L_c^3}{\nu^2}\mathrm{Pr} \tag{16}$$

where β is the coefficient of volume expansion ($\beta = 1/T$ for ideal gases), $\nu = \mu/\rho$ is the kinematic viscosity of the fluid (ρ is the density of the fluid and μ is the dynamic viscosity of the fluid), T_s is the temperature of the surface, T_∞ is the temperature of the fluid sufficiently far from the surface.

For forced air cooling, Nu can be expressed as [24]

$$\mathrm{Nu} = 0.3 + \frac{0.62\mathrm{Re}_L^{1/2}\mathrm{Pr}^{1/3}}{\left[1+\left(\frac{0.4}{\mathrm{Pr}}\right)^{2/3}\right]^{1/4}}\left[1+\left(\frac{\mathrm{Re}_L}{282000}\right)^{5/8}\right]^{4/5} \tag{17}$$

where Re_L is the Reynolds number. The critical Reynolds number for flow across a circular cylinder is about $\mathrm{Re_{cr}} = 2\times10^5$. That is, the boundary layer remains laminar for about $\mathrm{Re}_L < 2\times10^5$ and becomes turbulent for $\mathrm{Re}_L > 2\times10^5$

$$\mathrm{Re}_L = \frac{VL_c}{\nu} \tag{18}$$

where *V* is the maximum velocity that occurs within the tube bank.

The radiation thermal resistance between case *i* and ambience far from the surface is given by

$$R_{\mathrm{rad},ia} = \frac{1}{\sigma\varepsilon A(T_i^2+T_a^2)(T_i+T_a)}. \tag{19}$$

The parameters of Prandtl number (Pr), kinematic viscosity (ν), thermal conductivity (k), density (ρ), and dynamic viscosity (μ) are the properties of air at 1 atm pressure, which can be obtained from [24].

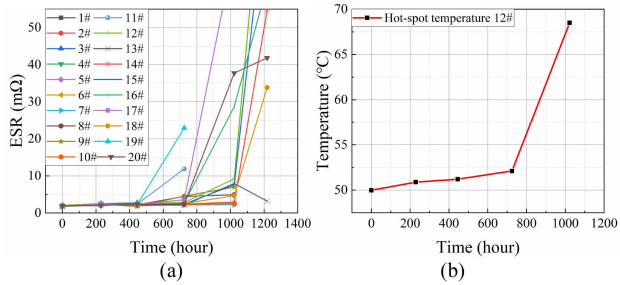

Fig. 4. Capacitor accelerated lifetime test results. (a) ESR aging curve. (b) Hot-spot temperature curve of 12#.

D. Effect of Aging on Thermal Field

According to the aging failure mechanism of capacitor, the self-healing breakdown and electrochemical corrosion inside the capacitor accumulate continuously. This results in an exponential increment in ESR, as is tested in an accelerated lifetime experiment, shown in Fig. 4(a) [26]. The aging model can be expressed as (2). The influence of ESR aging on capacitor temperature is shown in Fig. 4(b).

According to the power loss model, the ESR increase cause by aging can affect the hot spot temperature under specific operating condition by increasing the heat production. This influence mechanism is incorporated with the updated thermal modeling process by iterative operation, which can effectively improve the accuracy of hot-spot temperature prediction in a long-time scale.

E. Universal Analytical Thermal Modeling Process

To derive the steady-state temperature distribution of capacitor bank, a flowchart based on the state-space thermal model is provided as shown in Fig. 5. For given operating condition, power loss can be obtained through heat production modeling which contains aging model and power loss model. Then, the layout of the capacitor bank, the physical characteristics of an individual capacitor, and the fluid properties are initialized. Next, the thermal resistance matrix $\boldsymbol{A}$ can be established in specific layout and heat dissipation mode through heat transfer modeling, which consists of thermal coupling analysis and heat dissipation analysis.

After several iterations, the case temperature and hot-spot temperature will stabilize, and then the initial steady-state temperature distribution can be obtained. For long-time scale thermal modeling, the ESR increment caused by aging is also included in this iterative modeling process, through which the steady-state temperature distribution at any aging state can be estimated.

IV. Case Study

In order to experimentally verify the validity of the proposed high-resolution analytical thermal modeling method, a capacitor

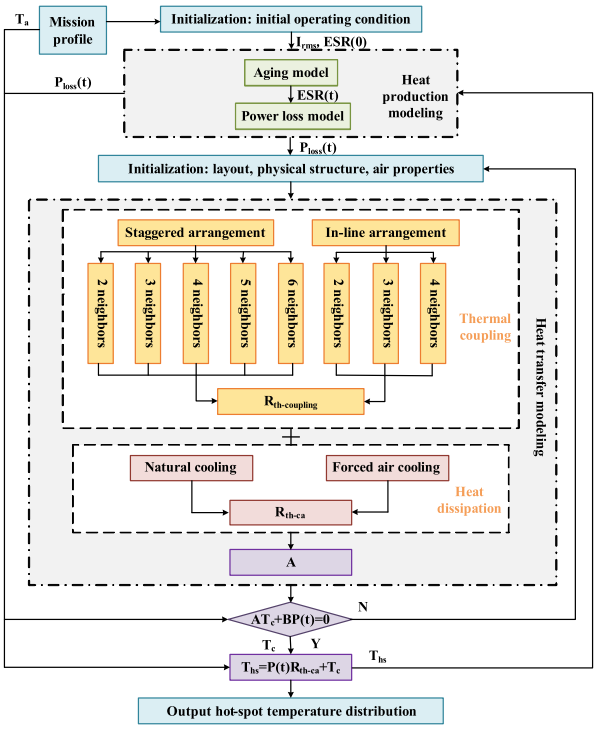

Fig. 5. Flowchart of updated thermal modeling process.

TABLE I
SPECIFICATIONS OF SINGLE CAPACITOR [27]

Parameters	Value
Rated DC voltage (V)	2000
Rated capacitance (μF)	6.8
ESR (mΩ)	10.6
Rth-hc (K/W)	3.2
Surface emissivity coefficient ε	0.09
Rated lifetime at 60°C (h)	350000
D (mm)	45
H (mm)	92
ST (mm)	50
SL (mm)	50

bank composed of nine single ones in which the thermocouples are buried in advance, used for temperature extraction. The specifications of single capacitor SRH-2000-6.8-B are given in Table I [27], where D is the diameter of capacitors, H is the height of the capacitors, ST is the transverse distance between two adjacent capacitors and SL is the longitudinal distance between two adjacent capacitors.

A. Experimental Platform

Nine capacitors are arranged as shown in Fig. 6. A 1600 Hz/20 A current is injected into the capacitor bank by a programable ac source (model AYF1307026 from ACTION) during the experiment. The ambient temperature is 23 °C. The fan provides adjustable wind speed and the maximum air velocity that occurs within the capacitor bank is 1 m/s. Fig. 7(a) and (b) shows the thermal images of capacitor bank under different cooling conditions by infrared camera.

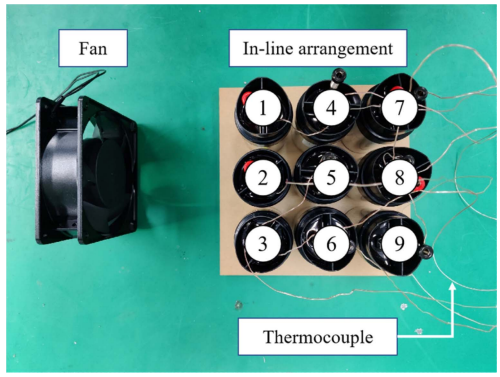

Fig. 6. Experimental platform of in-line design capacitor bank.

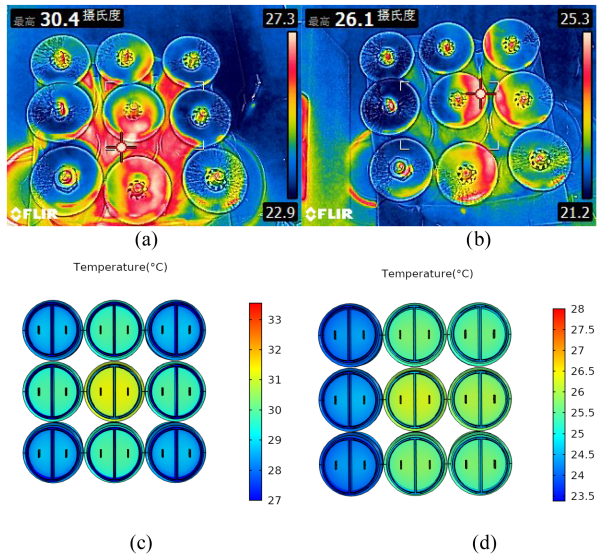

Fig. 7. Experimental results and FEM simulation results of in-line design. (a) Thermal images under natural cooling. (b) Thermal images under forced air cooling. (c) FEM simulation results of temperature distribution under natural cooling. (d) FEM simulation results of temperature distribution under forced air cooling.

B. Finite-Element Simulation

In order to prove the superiority of the proposed model, finite element simulation result is provided as a reference. In the software, the 3-D geometry of capacitors, and spatial arrangement of the bank are well defined referring to the actual dimension in Table I. The size of the rectangular wind channel is set to 0.25, 0.18, and 0.45 m in accordance with the width, height and depth; the inlet air velocity is set to 0.5 m/s and at the outlet and the normal stress is equal the outlet pressure; at all solid surfaces, the velocity is set to zero in all three spatial directions. In the steady thermal-fluid finite element model, the capacitor bank is set to heat transfer in solids, and the fluid channel is set to heat transfer in fluids, laminar flow.

The temperature distribution under natural cooling and forced air cooling obtained by FEM is shown in Fig. 7(c) and (d).

TABLE II
MEASURED PROPERTY OF AIR AT 1 ATM PRESSURE, 25 °C [24]

Parameters	Value
Thermal conductivity k (W/m·°C)	0.02551
Dynamic viscosity μ (kg/m·s)	1.849×10^{-5}
Prandtl Number (Pr)	0.7296
Density ρ (kg/m^2)	1.184
Kinematic Viscosity v (m^2/s)	1.562×10^{-5}

TABLE III
THE COMPARISON OF THE THERMAL SIMULATION METHODS

	Accuracy	Applicability	Computational Burden
1-D thermal network	+	+	+++
Thermal modeling method in [2]	++	++	++
FEM	+++	+++	+
Proposed method	+++	+++	++

Superior: +++, Intermediate: ++, Inferior: +.

TABLE IV
RESULTS COMPARISON UNDER NATURAL COOLING, IN-LINE DESIGN (°C)

Number	Experimental results	FEM results	Method in [2]	Proposed method	1-D model
1	30.9	31.2	28.9	30.6	26.5
2	31.7	32.3	29.4	32.1	26.5
3	29.8	31.2	28.9	30.6	26.5
4	31.5	32.3	29.4	32.1	26.5
5	33.5	33.5	30.1	33.8	26.5
6	30.7	32.3	29.4	32.1	26.5
7	31.1	31.2	28.9	30.6	26.5
8	31.5	32.3	29.4	32.1	26.5
9	30.8	31.2	28.9	30.6	26.5

TABLE V
RESULTS COMPARISON UNDER FORCED AIR COOLING, IN-LINE DESIGN (°C)

Number	Experimental results	FEM results	Proposed method
1	26.6	26.7	26.3
2	26.3	26.9	26.5
3	25.4	26.7	26.3
4	26.9	28.1	26.6
5	27.4	28.5	26.8
6	26.6	28.1	26.6
7	27.4	28.0	26.9
8	27.7	28.4	27.1
9	27.2	28.0	26.9

C. Model Verification

Assuming the capacitor bank is at standard atmospheric pressure, the property of air is given in Table II.

For natural cooling, the hot-spot temperature of each individual capacitor at different positions, is collected by experiment as shown in Appendix, Table IV. Parallelly, the hot-spot temperature simulation results obtained by FEM, 1-D simplified thermal network, thermal modeling method in [2] and proposed method are provided for comparison, as shown in Fig. 8.

For forced air cooling, the proposed thermal modeling method can also be applyed to obtain the hot-spot temperature, while neither of the conventional two methods can.Tests were carried out at different wind speeds, and the test results of 0.5 m/s are presented in Appendix, Table V and Fig. 9 as an example, compared with the experimental results and the FEM simulation results.

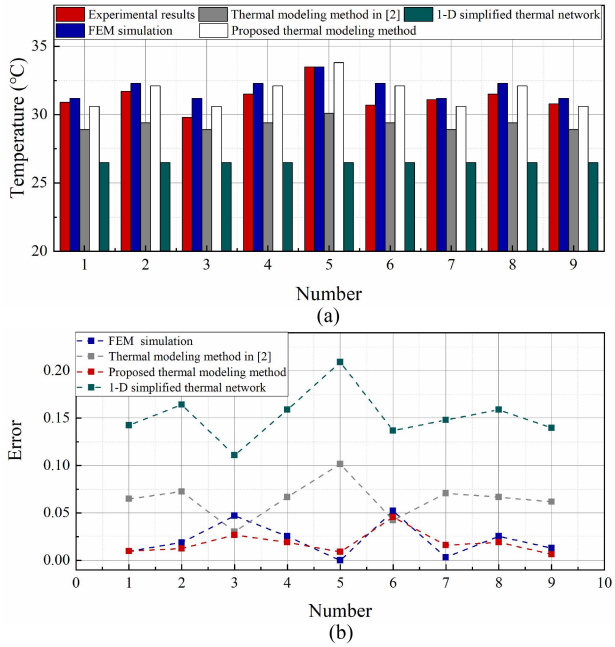

Fig. 8. Comparison of hot-spot temperature estimation results of in-line design among FEM, 1-D thermal network, thermal modeling method in [2] and proposed method under natural cooling. (a) Bar chart of result comparison. (b) Error analysis.

The error analysis of different methods in the two cooling modes is shown in Figs. 8(b) and 9(b). Obviously, by FEM simulation and the proposed thermal modeling method, the error is close to less than 5% under natural cooling. The accuracy is higher than the conventional two analytical thermal modeling methods and this meets better the demand of industrial applications. In addition, the proposed thermal modeling method fully considers the coupling mode of thermal field and fluid field under different heat dissipation conditions, and the application range of this method is extended. Under forced air cooling, as is shown in Fig. 9(b), the error is still less than 5%. In summary, the proposed thermal modeling method greatly improves the calculation speed in contrast with FEM and still keeps a good level of accuracy. Compared with the simulation time of more than 10 min for FEM, the proposed model only needs 3 s. This will greatly contribute to the reliability evaluation process.

V. DESIGN OPTIMIZATION OF CAPACITOR BANK

Under natural cooling, for the in-line designed capacitor bank, as mentioned previously in Section IV, the temperature distribution is heavily uneven. The hot-spot temperature of the central capacitor is much higher than that of the others. Such distribution is brought by different coupling effects on each individual capacitor. For capacitor banks serving in long-term, this uneven temperature distribution will lead to premature aging failure of the high-temperature ones, and then affect the reliability of the whole bank. In order to solve this problem, a new arrangement for capacitor bank is discussed in this section, in an attempt to reduce the temperature difference between individuals without changing the cooling mode or device dimension.

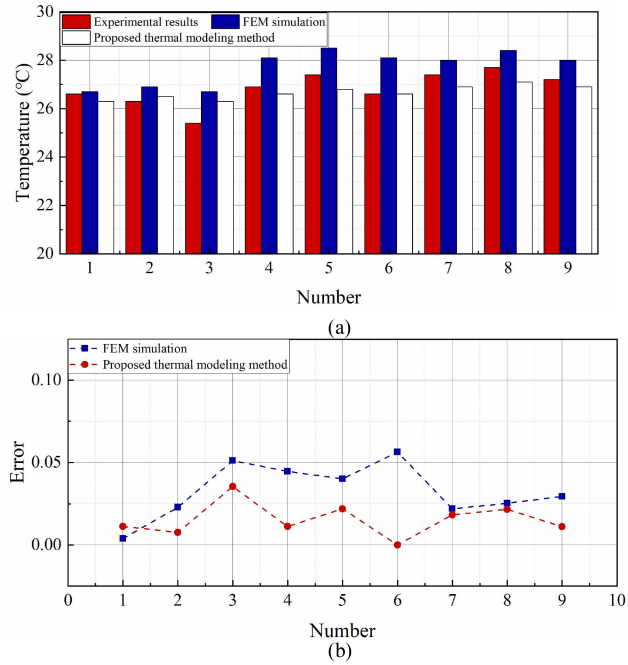

Fig. 9. Comparison of hot-spot temperature estimation result of in-line design among FEM, and proposed method under forced air cooling. (a) Bar chart of result comparison. (b) Error analysis.

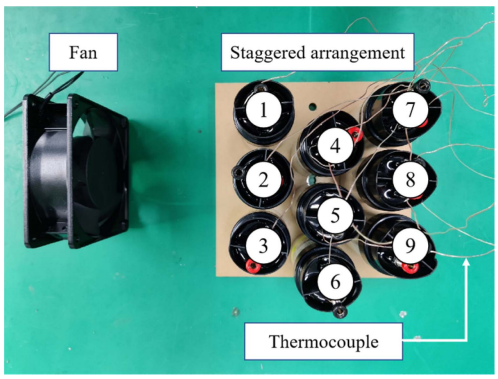

Fig. 10. Experimental platform of staggered design capacitor bank.

A. Staggered Arrangement

The new arrangement is staggered arrangement, as shown in Fig. 10. In this way, the adjacent capacitors of the middle one is changed from position 4 to 6, thus the heat dissipation condition is improved.

B. Simulation and Experimental Results

According to (10)–(19), the thermal resistance network of the new design is updated, then the modeling methods mentioned before are performed to derive the temperatures. Using the same experimental platform in Section IV, temperature extraction of the staggered capacitor bank is completed under the same operating condition. Fig. 11(a) and (b) shows the thermal images of capacitor bank under different cooling conditions in the staggered arrangement by infrared camera. The temperature distribution

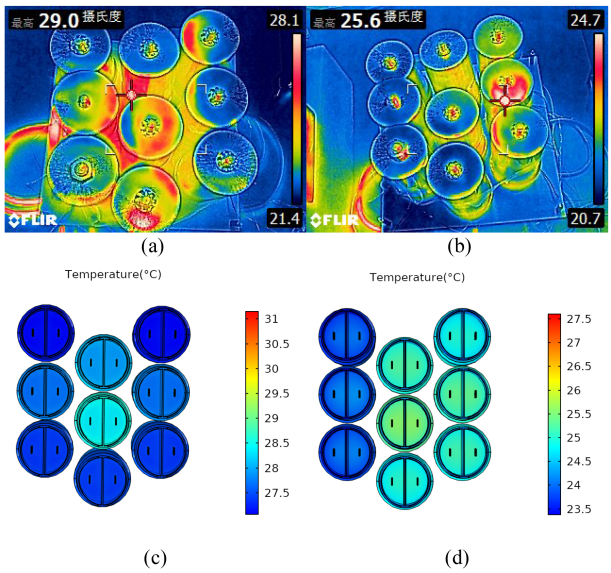

Fig. 11. Experimental results and FEM simulation results of staggered design. (a) Thermal images under natural cooling. (b) Thermal images under forced air cooling. (c) FEM simulation results of temperature distribution under natural cooling. (d) FEM simulation results of temperature distribution under forced air cooling.

TABLE VI
RESULTS COMPARISON UNDER NATURAL COOLING, STAGGERED DESIGN (°C)

Number	Experimental results	FEM results	Proposed method	1-D model
1	28.8	29.7	29.5	26.5
2	29.9	30.4	30.1	26.5
3	29.7	30.1	28.8	26.5
4	30.1	30.7	29.5	26.5
5	30.8	30.2	31.4	26.5
6	29.8	30.1	30.7	26.5
7	30.4	29.7	29.5	26.5
8	29.6	30.4	30.1	26.5
9	28.9	30.1	28.8	26.5

under natural cooling and forced air cooling obtained by FEM is shown in Fig. 11(c) and (d).

For natural cooling, hot-spot temperature data is collected as shown in Appendix, Table VI, still comparing FEM simulation, 1-D simplified thermal network, proposed thermal modeling method, and experimental results.

In this case, the average error of proposed method is less than 4%, staying at the same level with that of FEM. Corresponding bar chart and error analysis are presented in Fig. 12.

Furthermore, a comparison of temperature distribution regarding capacitor position is also shown in Fig. 13 between in-line arrangement and staggered arrangement under natural cooling. It is worth noting that, the average temperature and temperature fluctuation in staggered arrangement is relatively small, which is much lower than that of in-line arrangement capacitor bank under the same working condition.

The reliability curves of capacitor in middle and corner position, utilizing the proposed thermal modeling process in Section III are drawn in Fig. 14 by means of the reliability evaluation method proposed in article [20]. It reveals that the staggered

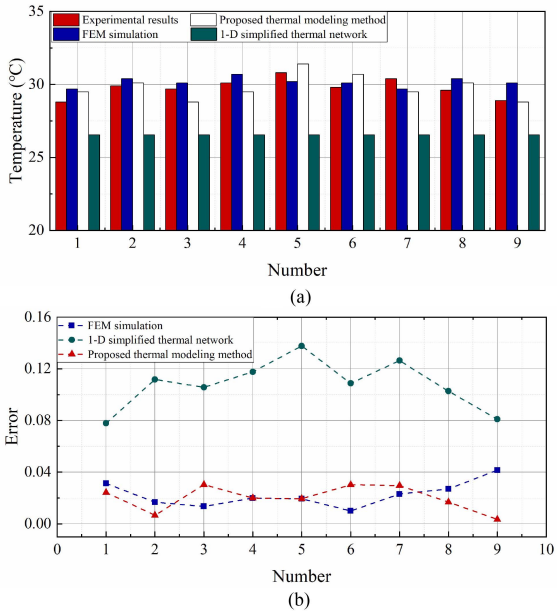

Fig. 12. Comparison of hot-spot temperature estimation result of staggered arrangement among FEM, 1-D thermal network and proposed method under natural cooling. (a) Bar chart of result comparison. (b) Error analysis.

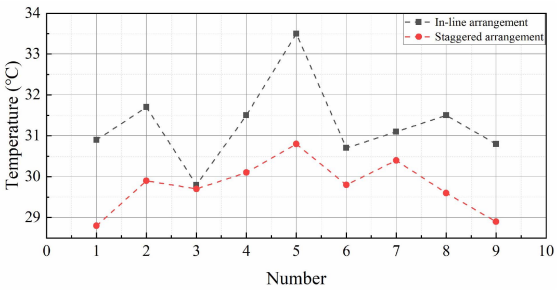

Fig. 13. Temperature distribution of the two design methods under natural cooling.

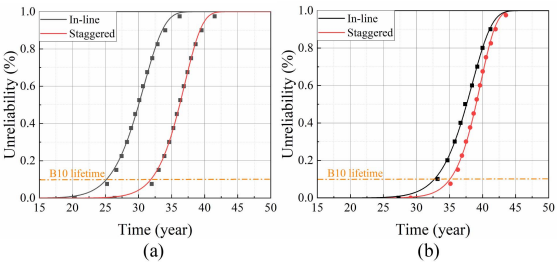

Fig. 14. Reliability curves of capacitors at two positions under different arrangement methods. (a) Middle position. (b) Corner position.

capacitor bank design is more efficient in heat dissipation and this could effectively improve the reliability of capacitors.

For forced air cooling, tests were carried out at different wind speeds. And the test results of 0.5m/s are similarly arranged in Appendix, Table VII and Fig. 15 as an example, relating to FEM simulation, the proposed method and experimental results.

The comparison between two design methods under this condition is also prepared in Fig. 16. It can be noticed that the temperature distribution of staggered bank design under forced air cooling do not show much difference with in-line arrangement.

TABLE VII
RESULT COMPARISON UNDER FORCED AIR COOLING, STAGGERED DESIGN (°C)

Number	Experimental results	FEM results	Proposed method
1	26.0	26.2	25.5
2	26.3	26.4	25.7
3	26.1	26.3	25.6
4	27.0	27.2	25.9
5	27.1	27.8	26.1
6	27.0	27.5	26.0
7	27.5	27.3	26.2
8	27.1	27.5	26.3
9	26.9	27.1	26.2

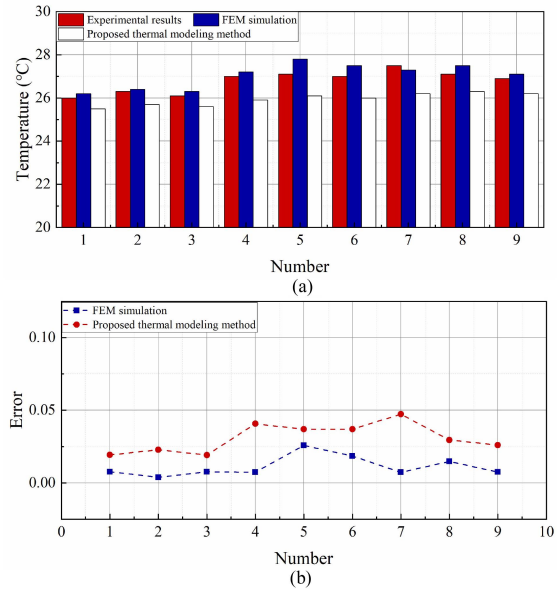

Fig. 15. Comparison of hot-spot temperature estimation result of staggered arrangement among FEM, conventional method and proposed model under forced air cooling. (a) Bar chart of result comparison. (b) Error analysis.

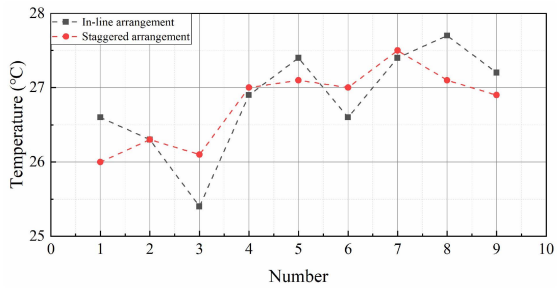

Fig. 16. Temperature distribution of the two design methods under forced air cooling.

C. Discussion

According to the experimental results of the different arranged capacitor banks under different heat dissipation conditions, a comprehensive performance comparison between the proposed method, 1-D thermal network, FEM, and other existing methods is given in Table III. Obviously, the proposed method has good performance in terms of accuracy, applicability and computational burden.

$$\boldsymbol{A}=\begin{bmatrix} -0.0963 & 0.0166 & 0 & 0.0166 & 0 & 0 & 0 & 0 & 0 & 0.0631 \\ 0.0166 & -0.0960 & 0.0166 & 0 & 0.0166 & 0 & 0 & 0 & 0 & 0.0462 \\ 0 & 0.0166 & -0.0963 & 0 & 0 & 0.0166 & 0 & 0 & 0 & 0.0631 \\ 0.0166 & 0 & 0 & -0.0960 & 0.0166 & 0 & 0.0166 & 0 & 0 & 0.0462 \\ 0 & 0.0166 & 0 & 0.0166 & -0.0960 & 0.0166 & 0 & 0.0166 & 0 & 0.0292 \\ 0 & 0 & 0.0166 & 0 & 0.0166 & -0.0960 & 0 & 0 & 0.0166 & 0.0462 \\ 0 & 0 & 0 & 0.0166 & 0 & 0 & -0.0963 & 0.0166 & 0 & 0.0631 \\ 0 & 0 & 0 & 0 & 0.0166 & 0 & 0.01660 & -0.0960 & 0.0166 & 0.0462 \\ 0 & 0 & 0 & 0 & 0 & 0.0166 & 0 & 0.0166 & -0.0963 & 0.0631 \end{bmatrix} \tag{A3}$$

VI. Conclusion

Due to the surging demand for high-resolution thermal analysis of capacitor banks in industrial applications, an analytical thermal modeling method considering complex cooling modes and device aging is proposed. The main conclusions are as follows.

1) The proposed improved thermal state-space modeling method, which offers better spatial and temporal resolution, can be used universally to describe the thermal behavior of multiheat source system under various heat dissipation modes.
2) The proposed thermal modeling method greatly improves the calculation speed on the premise of keeping the accuracy at a similar level to FEM simulation.
3) The proposed staggered arrangement prominently alleviates the uneven temperature distribution of conventional in-line arrangement of capacitor bank, guaranteeing the device reliability in long-term operation.

Appendix

1) *Derivation Details of the Coupling Thermal Resistance* $R_{\mathrm{th},ij}$

$R_{\mathrm{th},ij}$ consists of $R_{\mathrm{coup,cond},ij}$ and $R_{\mathrm{coup,rad},ij}$. For different cooling modes, the derivation methods of the $R_{\mathrm{th},ij}$ are the same.

$$R_{\mathrm{th},ij}=\frac{1}{\frac{1}{R_{\mathrm{coup,cond},ij}}+\frac{1}{R_{\mathrm{coup,rad},ij}}}. \tag{A1}$$

The derivation process of $R_{\mathrm{coup,cond},ij}$ and $R_{\mathrm{coup,rad},ij}$ are expressed as (10)–(12).

2) *Derivation Details of the Thermal Resistance From Case to Ambience* $R_{\mathrm{th},\ ia}$

$R_{\mathrm{th},ia}$ consists of $R_{\mathrm{conv},ia}$ and $R_{\mathrm{rad},ia}$. For different cooling modes, the derivation methods of the $R_{\mathrm{rad},\ ia}$ are the same. But the derivation methods of the $R_{\mathrm{conv},\ ia}$, are different.

$$R_{\mathrm{th},ia}=\frac{1}{\frac{1}{R_{\mathrm{conv},ia}}+\frac{1}{R_{\mathrm{rad},ia}}}. \tag{A2}$$

The derivation process of $R_{\mathrm{conv},\ ia}$ and $R_{\mathrm{rad},\ ia}$ are expressed as (13)–(19).

3) *Derivation Details of the Thermal Resistance Matrix* $\boldsymbol{A}$

After obtaining all the thermal parameters, the thermal resistance matrix $\boldsymbol{A}$ can be expressed as (8). Taking the in-line arrangement capacitor bank under natural cooling condition as an example, the $\boldsymbol{A}$ can be solved as (A-3) shown at the top of this page.

Then, the steady-state case temperature distribution can be solved by energy balance (7), letting $d\boldsymbol{T}_c/dt=0$.

References

[1] H. Wang and F. Blaabjerg, "Reliability of capacitors for DC-link applications in power electronic converters—An overview," *IEEE Trans. Ind. Appl.*, vol. 50, no. 5, pp. 3569–3578, Sep./Oct. 2014.

[2] H. Wang and H. Wang, "Analytical modeling and design of capacitor bank considering thermal coupling effect," *IEEE Trans. Power Electron.*, vol. 36, no. 3, pp. 2629–2640, Mar. 2021.

[3] S. Yang, A. Bryant, P. Mawby, D. Xiang, L. Ran, and P. Tavner, "An industry-based survey of reliability in power electronic converters," *IEEE Trans. Ind. Appl.*, vol. 47, no. 3, pp. 1441–1451, May/Jun. 2011.

[4] V. Belko, D. Glivenko, O. Emelyanov, I. Ivanov, and A. Plotnikov, "Current pulse polarity effect on metallized film capacitors failure," *IEEE Trans. Plasma Sci.*, vol. 45, no. 6, pp. 1020–1025, Jun. 2017.

[5] R. W. Brown, "Linking corrosion and catastrophic failure in low-power metallized polypropylene capacitors," *IEEE Trans. Device Mater. Rel.*, vol. 6, no. 2, pp. 326–333, Jun. 2006.

[6] B. Peng, F. Lin, H. Li, Y. Chen, M. Zhang, and F. Lv, "Calculation and measurement of metalized film capacitor's inner pressure and its influence on self-healing characteristics," *IEEE Trans. Dielect. Elect. Insul.*, vol. 17, no. 5, pp. 1612–1618, Oct. 2010.

[7] Z. Li et al., "Lifetime prediction of metallized film capacitors based on capacitance loss," *IEEE Trans. Plasma Sci.*, vol. 41, no. 5, pp. 1313–1318, May 2013.

[8] H. Wang et al., "Transitioning to physics-of-failure as a reliability driver in power electronics," *IEEE J. Emerg. Sel. Topics Power Electron.*, vol. 2, no. 1, pp. 97–114, Mar. 2014.

[9] M. Makdessi, A. Sari, and P. Venet, "Metallized polymer film capacitors ageing law based on capacitance degradation," *Microelectronics Rel.*, vol. 54, no. 9-10, pp. 1823–1827, Sep. 2014.

[10] D. Zhou, H. Wang, and F. Blaabjerg, "Mission profile based system-level reliability analysis of DC/DC converters for a backup power application," *IEEE Trans. Power Electron.*, vol. 33, no. 9, pp. 8030–8039, Sep. 2018.

[11] Q. Sun, J. Zhou, Z. Zhong, J. Zhao, and X. Duan, "Gauss-poisson joint distribution model for degradation failure," *IEEE Trans. Plasma Sci.*, vol. 32, no. 5, pp. 1864–1868, Oct. 2004.

[12] A. Jezierska, C. Chaux, J. Pesquet, H. Talbot, and G. Engler, "An EM approach for time-variant poisson-gaussian model parameter estimation," *IEEE Trans. Signal Process.*, vol. 62, no. 1, pp. 17–30, Jan. 1, 2014.

[13] Y. Cho, T. LaBella, and J. -S. Lai, "A three-phase current reconstruction strategy with online current offset compensation using a single current sensor," *IEEE Trans. Ind. Electron.*, vol. 59, no. 7, pp. 2924–2933, Jul. 2012.

[14] H. Wang, C. Li, G. Zhu, Y. Liu, and H. Wang, "Model-based design and optimization of hybrid DC-link capacitor banks," *IEEE Trans. Power Electron.*, vol. 35, no. 9, pp. 8910–8925, Sep. 2020.

[15] R. Yao, H. Li, W. Lai, A. S. Bahman, and F. Iannuzzo, "Lifetime analysis of metallized polypropylene capacitors in modular multilevel converter based on finite element method," *IEEE J. Emerg. Sel. Topics Power Electron.*, vol. 9, no. 4, pp. 4248–4259, Aug. 2021.

[16] Y. j. Ko, H. Jedtberg, G. Buticchi, and M. Liserre, "Analysis of DC-link current influence on temperature variation of capacitor in a wind turbine application," *IEEE Trans. Power Electron.*, vol. 33, no. 4, pp. 3441–3451, Apr. 2018.

[17] M. Makdessi, A. Sari, P. Venet, P. Bevilacqua, and C. Joubert, "Accelerated ageing of metallized film capacitors under high ripple currents combined with a DC voltage," *IEEE Trans. Power Electron.*, vol. 30, no. 5, pp. 2435–2444, May 2015.

[18] D. Zhou, Y. Song, Y. Liu, and F. Blaabjerg, "Mission profile based reliability evaluation of capacitor banks in wind power converters," *IEEE Trans. Power Electron.*, vol. 34, no. 5, pp. 4665–4677, May 2019.
[19] H. Wang et al., "Lifetime prediction of DC-link capacitors in multiple drives system based on simplified analytical modeling," *IEEE Trans. Power Electron.*, vol. 36, no. 1, pp. 844–860, Jan. 2021.
[20] C. Lv, J. Liu, Y. Zhang, W. Lei, R. Cao, and G. Lv, "Reliability modeling for metallized film capacitors based on time-varying stress mission profile and aging of ESR," *IEEE J. Emerg. Sel. Topics Power Electron.*, vol. 9, no. 4, pp. 4311–4319, Aug. 2021.
[21] B. Sun, X. Fan, C. Qian, and G. Zhang, "PoF-simulation-assisted reliability prediction for electrolytic capacitor in LED drivers," *IEEE Trans. Ind. Electron.*, vol. 63, no. 11, pp. 6726–6735, Nov. 2016.
[22] Y. Ran, Z. Meimei, L. Hui, L. Wei, W. Xiao, and L. Haiyang, "Reliability modeling and analysis on metallized film capacitors for MMC," in *Proc. 10th Int. Conf. Power Electron. ECCE Asia*, 2019, pp. 1854–1860.
[23] TDK EPCOS, "Film capacitors, power electronic capacitors, B2562," TDK EPCOS, Munich, Germany, 2022, [Online]. Avaliable: https://www.tdk-electronics.tdk.com/inf/20/50/ds/B2562_.pdf
[24] Y. A. Cengel and A. J. Ghajar, *Heat and Mass Transfer: Fundamentals and Applications*, 4th ed., New York, NY, USA: McGraw Hill, 2011, pp. 90–833.
[25] R. Siegel and J. O. Howell, *Thermal Radiation Heat Transfer*, 2nd ed., Washington, DC, USA: Hemisphere Publ. Corp., 1982, pp. 172—-273.
[26] C. Lv, J. Liu, Y. Zhang, W. Lei, and R. Cao, "An improved lifetime prediction method for metallized film capacitor considering harmonics and degradation process," in *Microelectronics Reliability*, vol. 114, Nov. 2020, Art. no. 113892.
[27] "Type SHP polypropylene, DC link capacitors, general technical characteristics," EACO, Neptune Beach, FL, USA, 2022, [Online]. Available: http://www.eaco.com/uploads/soft/160630/SRH.pdf
[28] "Type 947D polypropylene, high energy density, DC link capacitors," Cornell Dubilier, New Bedford, MA, USA, 2022, [Online]. Avaliable: http://www.cde.com/resources/catalogs/947D.pdf

Chunlin Lv (Graduate Student Member, IEEE) received the B.S. degree in electrical engineering from Chongqing University, Chongqing, China, in 2018. He is currently working toward the Ph.D. degree in electrical engineering with Xi'an Jiaotong University, Xi'an, China.

His research interests include reliability modeling of capacitors, reliability evaluation of power electronic systems and optimization design of power electronic systems.

Jinjun Liu (Fellow, IEEE) received the B.S. and Ph.D. degrees in electrical engineering from Xi'an Jiaotong University (XJTU), Xi'an, China, in 1992 and 1997, respectively.

He was a Faculty at the XJTU Electrical Engineering School. From late 1999 to early 2002, he was at the Center for Power Electronics Systems, Virginia Polytechnic Institute and State University, Blacksburg, VA, USA, as a Visiting Scholar. In late 2002, he was promoted to a Full Professor and then the Head of the Power Electronics and Renewable Energy Center at XJTU, which now comprises more than 20 faculty members and more than 200 graduate students and carries one of the leading power electronics programs in China. From 2005 to early 2010, he was an Associate Dean at the Electrical Engineering School, XJTU, and from 2009 to early 2015, he was the Dean for Undergraduate Education of XJTU. He is currently a XJTU Distinguished Professor of Power Electronics. He coauthored 3 books (including one textbook), published more than 500 technical papers in peer-reviewed journals and conference proceedings, holds more than 70 invention patents (China/US/EU), and delivered for many times plenary keynote speeches and tutorials at IEEE conferences or China national conferences. His research interests include modeling, control, and design methods for power converters and electronified power systems, power quality control and utility applications of power electronics, and microgrids for sustainable energy and distributed generation.

Dr. Liu was the recipient of for many times governmental awards at national level or provincial/ministerial level for scientific research/teaching achievements. He was also the recipient of the 2006 Delta Scholar Award, the 2014 Chang Jiang Scholar Award, the 2014 Outstanding Sci-Tech Worker of the Nation Award, the 2016 State Council Special Subsidy Award, the IEEE Transactions on Power Electronics 2016 and 2021 Prize Paper Awards, the Nomination Award for the Grand Prize of 2020 Bao Steel Outstanding Teacher Award, and the 2022 Fok Ying Tung Education and Teaching Award. He was the IEEE Power Electronics Society Region 10 Liaison and then China Liaison for 10 years, has been an Associate Editor for IEEE TRANSACTIONS ON POWER ELECTRONICS since 2006, from 2015–2019, he was the Executive Vice President and during 2020–2021, he was the Vice President of IEEE PELS. He was on the Board of China Electrotechnical Society 2012-2020 and was elected the Vice President in 2013 and the Secretary General in 2018 of the CES Power Electronics Society. From 2013 to 2021, he was the Vice President for International Affairs, China Power Supply Society, and since 2016, he has been the inaugural Editor-in-Chief of *CPSS Transactions on Power Electronics and Applications*. He was elected the President of CPSS in Nov. 2021. Since 2013, he has been the Vice Chair of the Chinese National Steering Committee for College Electric Power Engineering Programs.

Yan Zhang (Member, IEEE) received the Ph.D. degree in electrical engineering from Xi'an Jiaotong University (XJTU), Xi'an, China, in 2014.

He is currently an Associate Professor with the School of Electrical Engineering, XJTU. From early 2016 to 2017, he was a Postdoctoral Research Fellow with the Department of Electrical and Computer Engineering, Queen's University, Kingston, ON, Canada. He has presided over research projects of the National Natural Science Foundation, the China Postdoctoral Science and Province Foundation, and the State Key Laboratory Foundation. He has authored or coauthored more than 50 technical papers in peer reviewed journals and conference proceedings and holds 10 China issued invention patents. His research interests include topology, model and control of power electronic systems, high-efficiency resonant power converters, and power electronics equipment reliability.

Jinpeng Yin received the B.S. and M.S. degrees in electrical engineering from Xi'an Jiaotong University, Xi'an, China, in 2019 and 2022, respectively.

His research interests include reliability modeling of capacitors, and the use of finite element method in reliability evaluation.

Xiaotong Zhang was born in Shaanxi, China in 1992. She received B.S. and M.S. degrees in electrical engineering in 2015 and 2018, respectively, from Xi'an University of Technology, Xi'an, China, where she is currently working toward the Ph.D. degree in electrical engineering with the State Key Laboratory of Electrical Insulation and Power Equipment.

Her major research fields are thermal management and insulation materials of power electronics.